



Morphological response to climate-induced flood-event variability in a subarctic river

Linnea Blåfield¹, Carlos Gonzales-Inca¹, Petteri Alho^{1,2}, and Elina Kasvi¹

¹Department of Geography and Geology, University of Turku, Turku, Finland

²Finnish Geospatial Research Institute FGI, National Land Survey of Finland, Espoo, Finland

Correspondence: Linnea Blåfield (linnea.m.blafield@utu.fi)

Received: 3 December 2024 – Discussion started: 7 January 2025

Revised: 6 June 2025 – Accepted: 27 June 2025 – Published: 10 September 2025

Abstract. This study examined the effects of climate-induced flood-event variability and peak sequencing on morphological response and sediment transport hysteresis patterns in a subarctic river. We classified 32 years of discharge hydrographs from a subarctic river according to their spring flood hydrograph shapes and peak sequences. These classified flood-event types and their frequencies were statistically analysed against seasonal and annual climatic conditions from the corresponding time periods. Morphodynamic modelling was employed to examine the effects of flood-event hydrograph shape and sequencing on morphological response and sediment transport hysteresis patterns during floods. The findings highlight the critical role that hydrograph shape and sequencing play in influencing river morphology and sediment transport dynamics, as each flood-event type produced distinct sediment transport hysteresis patterns and morphological outcomes. Variance and trend analyses revealed that prevailing climatic conditions significantly influence the hydrograph shapes of spring flood events. Annual mean temperature, total precipitation, and snow accumulation, together with cold season mean temperature, spring rainfall, and May cumulative temperature, had the greatest effect on the type of spring flood event observed. Significant increasing trends were identified in annual and spring mean temperatures, spring rainfall, and the frequency of rain-on-snow events. This suggests that ongoing climatic shifts are actively modifying the nature of spring flood events, favouring more complex and variable hydrograph forms. Consequently, future sediment transport and morphological evolution in subarctic rivers are likely to become increasingly event-driven, less predictable, and more sensitive to interannual climatic variability. These changes emphasize the need for adaptive management strategies that can accommodate the emerging hydrological and geomorphological dynamics under a changing climate.

Highlights.

- Sediment transport hysteresis pattern is dependent on the number and volume of flood peak sequences.
- Flood-event type significantly affects river morphological response.
- Increase of multi-peaking flood events, mean temperature, and changing precipitation patterns affects the future river system stability.
- Hydrograph shape can be associated to specific preceding climatic conditions.

1 Introduction

Hydrological variability significantly affects riverine sediment fluxes, especially in cold climate rivers where sediment transport is highly seasonal, occurring predominantly during spring floods (Syvitski, 2002; Favaro and Lamoureux, 2015; Zhang et al., 2022). Snowmelt-driven spring floods carry the majority of the annual sediment budget and therefore, they define the timing and volume of sediment transport and ultimately the whole river morphology. Currently, cold climate rivers are experiencing rapid shifts in hydroclimatic conditions, influencing the flow-sediment interaction in the river systems (Meriö et al., 2019; Beel et al., 2021; Li

et al., 2021; Zhang et al., 2023; Blåfield et al., 2024a). As hydroclimatic conditions evolve, the characteristics of flood events are also changing with implications to the traditional sediment transport dynamics. For instance, the shift in the snow-to-precipitation ratio and changes in the timing and intensity of snowmelt have already altered flood hydrographs i.e. the shape, magnitude, duration, and sediment transport capacity of events in cold-climate rivers (Wohl, 2017; Gohari et al., 2022; Hopwood et al., 2018; Zhang et al., 2022; Blåfield et al., 2024a; Lintunen et al., 2024). Flood-events are usually classified by their generating processes (e.g. intense precipitation, snowmelt, rain-on-snow, ice jamming, dam break etc.), with less emphasis on the event type and sequences itself. Previous studies (Viglione et al., 2010; Fischer and Schumann, 2020; Gohari et al., 2022), however, have reported that ongoing regime shifts have altered flood-event shapes. Over the past century, multi-peaking floods have become more common, not only in central Europe, but also in high-latitude regions.

In multi-peaking floods, the order and duration of different peaks significantly affects the sediment transport volume and the pattern of sediment transport hysteresis (Mao, 2018). Therefore, understanding the contribution of flood-event sequences to sediment transport is crucial for predicting the effect of climate change on fluvial sediment dynamics and the morphological response of river systems (Mao, 2012; Karimae Tabarestani and Zarrati, 2015). This is particularly important in cold-climate rivers, which have historically experienced a single major snowmelt-driven flood and low sediment loads. However, due to hydroclimatic regime shifts, altered fluvial dynamics, and possible permafrost or glacier melt, these regions are increasingly becoming hotspots for elevated sediment transport (Syvitski, 2002; Li et al., 2021; Zhang et al., 2022). Recent studies indicate that migration rates of large, sinuous rivers in the Arctic permafrost region have slowed by 20 % during the past 50 years due to decreased fluvial energy and increased bank shrubification (Ielpi, 2023). Contrasting findings have been made on the Tibetan Plateau where migration rates have increased by 34 % due to increased discharge volumes and river bank destabilization caused by permafrost melt (Sha et al., 2025). In boreal-subarctic regions, where the focus of this study is, the fluvial activity and extreme discharge events outside the spring flood season have increased while spring flood peaks have decreased significantly (Korhonen and Kuusisto, 2010; Lintunen et al., 2024). The increased fluvial activity outside traditional flood season is caused by an increasing number of extreme rainfall events (Nikulin et al., 2011) which are intensifying bank erosion and sediment transport (Kärkkäinen and Lotsari, 2022). However, the annual total volume of water has not yet changed (Lintunen et al., 2024). All these findings suggest that climate change has diverse effects on fluvial dynamics across the high-latitude region, and therefore more attention should be focused on sediment transport dynamics and the hysteresis pattern under evolving discharge

conditions. Understanding these processes is essential because sediment transport not only shapes river morphology but also governs aquatic habitats, influences nutrient fluxes, and affects infrastructure stability.

One effective way to evaluate the sediment transport process and morphological response of the river channel is through analysis of sediment transport hysteresis patterns, which reflect the sediment transport affected by riverbed structure, sediment composition, and availability at different stages of the flow hydrograph (Williams, 1989; Reesink and Bridge, 2011; Gunsolus and Binns, 2018). In cold climate rivers various types of sediment transport hysteresis have been observed due to highly seasonal and varying sediment availability between catchments (Vatne et al., 2008; Kociuba, 2021; Wenng et al., 2021; Zhang et al., 2021; Liébault et al., 2022). Yet, measuring bedload and hysteresis in natural rivers during high flows remains challenging and is prone to biases. As a result, long time series of bedload transport and hysteresis are scarce worldwide (Mao, 2018; Zhang et al., 2023). Thus, we rely on laboratory experiments, computational modelling, and field measurements of suspended load when evaluating and measuring the current, and predicting the future sediment fluxes and morphodynamic response of the river channels.

The ability to evaluate and predict the effects of climate change on sediment transport rates and morphological response is essential not only for understanding fluvial morphodynamics, such as channel stability and sediment connectivity but also for a wide range of river engineering and management applications (Mao, 2018; Gupta et al., 2022; Najafi et al., 2021). Therefore, this study aims to (i) analyse and classify the variation in flood-event hydrographs over the past 32-years in a subarctic river, (ii) link the flood events to seasonal and annual climate conditions, and (iii) evaluate the channels morphological response distinctive to each flood-event type utilizing morphodynamic modelling and sediment transport hysteresis analysis. We expect to detect linkages between the flood-event hydrograph shape and climatic conditions as well as diverse patterns of morphological response and sediment transport hysteresis. The study was conducted on a river reach in Finland, located at 70° N latitude. Despite its high latitude, Finland has a relatively mild climate compared to other regions at similar latitudes, such as Siberia, northern Canada, and Alaska, largely due to the warming influence of the Gulf Stream and the North Atlantic Drift. As a result, Finland is mostly free of permafrost (Luoto et al., 2004), although small areas of permafrost exist in the form of *palsa* mires. These *palsas* are primarily found in north-western Finland (Seppälä, 1997; Gislén et al., 2017; Verdonen et al., 2023). Nevertheless, Finland experiences seasonally frozen ground for periods ranging from four (South) to eight (North) months each year (Rimali, 2019).

2 Study area

The meandering and unregulated Pulmanki River is located in northern Finland (Fig. 1a). The river is a tributary of the Tana River which flows into the Arctic Ocean on the Norwegian side of the border (Fig. 1a). The river is divided into two separate sections by Lake Pulmankijärvi (Fig. 1b). The area of interest in this study is a 6 km long reach on the upper course of the Pulmanki River approximately 13 m above mean sea level (Fig. 1b). This reach consists of 13 meander bends with a reach sinuosity of 2.4. The bankfull width of the river varies between 60 to 100 m, depending on the valley confinement. The river flows through glaciolacustrine and glacio-fluvial sediments deposited on the fjord bottom after the final wasting of the Fennoscandian ice sheet (Mansikkaniemi, 1967; Hirvas et al., 1988; Johansson, 2007). The D50 value of the channel bed material ranges from 0.1 to 4 mm and a sandy bedload (D50 0.43 mm) dominates the sediment transport. The amount of suspended material is minimal ($0\text{--}180\text{ mg L}^{-1}$), even during the spring flood (Lotsari et al., 2020). The bed morphology is typical for sand bed rivers and consists of dunes, ripples, pools, and riffles, the bed is unvegetated and mobile through the year. The channel is frozen from October to May, and the seasonal discharge ranges from 0.5 to $100\text{ m}^3\text{ s}^{-1}$. A spring flood generated by the snowmelt occurs annually in late-May or early June. Lower discharge peaks are associated with precipitation events during July, August, and September. The river belongs to the subarctic-nival hydrological regime (Lininger and Wohl, 2019) and to the Köppen climate class: “Cold, without dry season, but with cold summer”, as the area is affected by the great Asian continent and both the Atlantic Ocean and the Gulf Stream. Based on the Nordic permafrost model by Gislås et al. (2017) the majority of the catchment is permafrost free (Fig. 1c). The south-western corner has 10 %–50 % probability of sporadic permafrost according to the model results based on land cover, snow accumulation, and temperature data. However, no confirmed field observations of sporadic permafrost from the area exist, and therefore we consider this catchment and river system as a non-permafrost river.

3 Data and methods

Discharge hydrographs of the years 1992–2023 were analysed and classified to recognize variability in spring flood-event shapes. The most typical flood event of each hydrograph type was selected for morphodynamic modelling to evaluate the channel morphodynamic response and sediment transport dynamics. The flood events extracted from the classified hydrographs were linked with climate data from the equivalent time period to examine possible connections between climate and flood-event shapes. The Mann–Kendall (M–K) trend test was run on the hydroclimatic variables to detect possible trends in the time series. Continuous dis-

charge and water level (WL) monitoring has been conducted in Pulmanki River since 2008 during open water season (May–September). The Pulmanki River discharge time series was complemented with Polmak discharge station data from Tana River (Fig. 1) to cover the whole 32-year time period. Sediment and bedload transport samples were collected during the spring and autumn field campaigns from various discharge conditions.

3.1 Hydrograph measurements and generation

Hydrographs of open water season were generated utilizing a combination of data sources. For the years 2008–2023, rating curves based on a combination of field data were generated: water pressure sensor data (LeveLogger 5, Solinst), WL data measured with Virtual Reference Station-Global Navigation Satellite System (VRS-GNSS), and discharge data measured with Acoustic Doppler Current Profiler (ADCP M9, Sontek). Each year, the water pressure sensors were placed into the upper Pulmanki River after ice breakup in spring and picked up before winter (see locations in Fig. 1). In this way the sensors covered the whole open water season and seasonal variations of water pressure, WL, and discharge at 15 min intervals. The location of the sensors was identical each year. To compensate for atmospheric influence on water pressure, air pressure sensor data from Solinst Barologger was subtracted from the water pressure readings. During field campaigns in May and September WL and discharge were measured daily from the LeveLogger locations for creating rating curves between LeveLogger pressure, WL, and discharge (Q). Based on the rating curves, a third-order polynomial function was selected for calculating annual hydrographs of open water seasons (Fig. 2a).

For the years 1992–2007, openly available daily discharge data from Polmak measurement station, maintained by the Norwegian Water Resources and Energy Directorate (NVE) were used. The station is located in the main channel of Tana River at the spot where Pulmanki River discharges into Tana (see Fig. 1, Q station number 3), and has been operating since November 1991. The discharge for Pulmanki River was derived from the Polmak station data using a rating curve and third-order polynomial function between the Polmak station discharge (Q) and Pulmanki River Q of 2008–2023 derived from the LeveLoggers (Fig. 2b). The final hydrographs of Pulmanki river are based on these two equations and data sources. The hydrographs were validated against ADCP discharge measurements from Pulmanki River main channel. These measurements were excluded from the rating curve creation. See the details of error metrics listed in Table 1.

3.2 Hydrograph classification

The hydrographs were classified into distinct flood-event types based on the peak shape in a Python program using the SciPy Scientific Python (SciPy) library. A threshold value

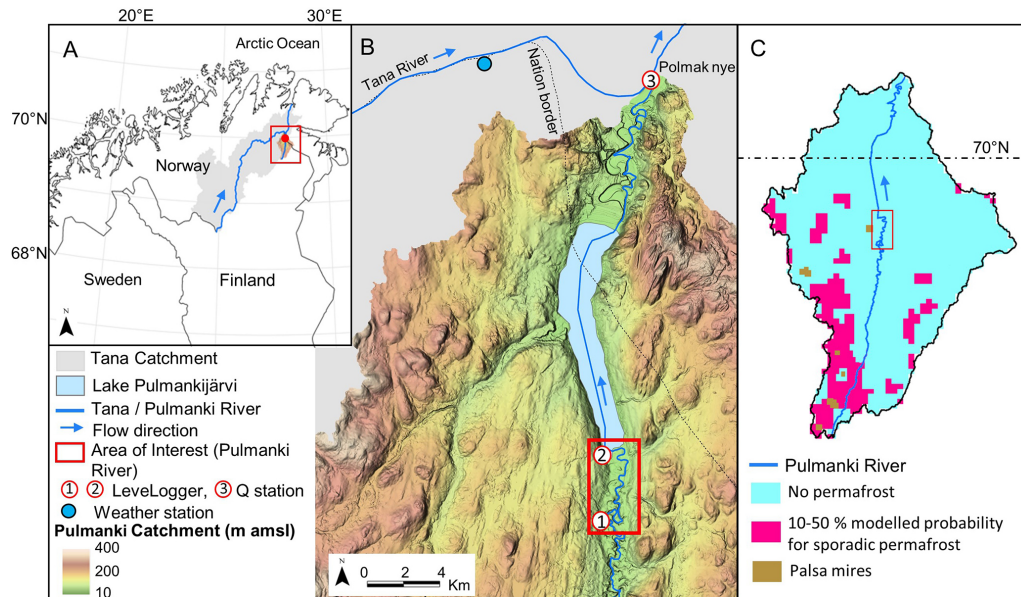


Figure 1. Area of interest. (a) The study area's location in the Northern most Finland. (b) Model area is marked with rectangle, and the locations of LeveLogger sensors (LL), discharge (Q), and weather station with circular markers. (c) The probability of sporadic permafrost within the catchment based on the Nordic permafrost model by Gissén et al. (2017). Pulmanki catchment 2×2 m DEM by National Land Survey of Finland.

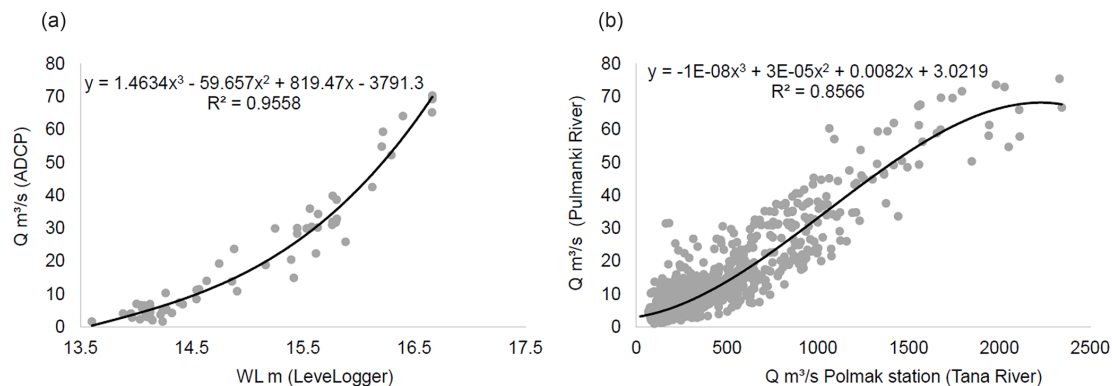


Figure 2. Rating curves for Pulmanki River hydrographs. (a) Regression curve of discharge measurements (Q $\text{m}^3 \text{s}^{-1}$ ADCP) and LeveLogger WL in Pulmanki River 2008–2023. This polynomial function A was used to calculate hydrographs for years 2008–2023 (b) Regression curve showing the relationship between the discharge in Pulmanki (Q $\text{m}^3 \text{s}^{-1}$) calculated based on regression curve (a) and Polmak (Q $\text{m}^3 \text{s}^{-1}$ measured, national gauging station) during 2008–2023. This polynomial function (b) was used for calculating Pulmanki River discharge for years 1992–2007.

of $23.46 \text{ m}^3 \text{s}^{-1}$ (75th percentile, p75 discharge) for flooding was set to classify significant spring flood events. A sensitivity analysis on peak-finding thresholds was conducted using the 50th, 60th, 70th, 80th, and 90th percentiles. Threshold values at the 70th and 80th percentiles were found to capture the majority of relevant spring flood events, and consequently, the 75th percentile (p75) was selected for this study. The commonly used threshold of the 90th percentile ($Q > 58 \text{ m}^3 \text{s}^{-1}$ in this case) restricted the dataset too severely, with the algorithm failing to detect spring floods in certain years, particularly those with low peak discharges. Further-

more, using the p90 value resulted in hydrographs that included only the very peak of the flood event, without capturing the rising and falling limbs of the hydrograph, which are crucial for evaluating sediment dynamics and flow–sediment interactions. Thresholds below the 70th percentile included peaks outside the spring flood season, and thus these thresholds were not ideal for this study. The definition for high and low flood event was set to be either above or below the mean flood discharge of $40 \text{ m}^3 \text{s}^{-1}$, respectively.

The event classification was done by estimating different flood peak features such as peak timing, promi-

Table 1. Error metrics of the final hydrographs derived from two different data sources: LeveLogger discharge data and Polmak Station discharge data. MAE = mean absolute error, SDE = standard deviation of error, r = correlation coefficient, n = number of samples.

Pulmanki River Q Derived from	Min Error ($\text{m}^3 \text{s}^{-1}$)	Max Error ($\text{m}^3 \text{s}^{-1}$)	Mean Error ($\text{m}^3 \text{s}^{-1}$)	MAE ($\text{m}^3 \text{s}^{-1}$)	SDE ($\text{m}^3 \text{s}^{-1}$)	r	R^2	n
LeveLogger	−9.59	10.73	−0.24	2.92	3.74	0.94	0.89	152
Polmak Station	−51.48	20.34	−0.39	2.59	4.65	0.89	0.80	1804

nence, peak height, and event duration. First, a Savitzky–Golay smoothing filter was applied to the dataset to reduce noise and enhance the detectability of flood peaks. This was accomplished using the `Savgol_filter` function from the “`scipy.signal`” module, with a window size of 11 and a polynomial order of three to preserve relevant hydrograph features. Peak shapes within the smoothed data were identified and classified into distinct flood events using the “`find_peaks`” function from the `scipy.signal` module. The following parameters and minimum values were found to most effectively identify peak events: the minimum discharge threshold for a flood event, defined as the 75th percentile ($p75\ Q$), a minimum hydrograph width of one day, measured from the start of the rising limb to the end of the recession limb, and a minimum prominence of $2 \text{ m}^3 \text{s}^{-1}$, indicating how much the peak stands out from the surrounding baseline.

Four different event types were detected: (a) High one-peak ($Q > 40 \text{ m}^3 \text{s}^{-1}$), (b) Low one-peak ($Q < 40 \text{ m}^3 \text{s}^{-1}$), (c) Two separate peaks ($Q > p75$, $Q < p75$, $Q > p75$), and (d) Wavy peak (two $Q > p75$ peaks) (Fig. 3a–d). For modelling purposes, the most typical event of each type was selected (red solid line in Fig. 3a–d). The precipitation-driven discharge peaks in July, August, and September were left out of the analysis as none of them exceed the flood threshold discharge of $p75$. In addition, previous studies indicate that the majority of high-latitude rivers transport most of their annual sediment load during the main flood event, i.e. the spring flood (Syvitski, 2002; Zhang et al., 2022; Blåfield et al., 2024b). Therefore, the focus of this study was placed solely on spring flood peaks. In this region, spring flood peaks are driven by climatic factors such as rising temperatures and rainfall, which induce snowmelt, increase runoff, and lead to the breakup of river ice cover.

3.3 Hydroclimatic data and statistical analysis

Climate data from the Nuorgam weather station (see location in Fig. 1b), 11 m above mean sea level and 17 km North of the Pulmanki River study area, was downloaded from the Finnish Meteorological Institute open data service. Daily total, min, mean and max temperature, precipitation, and snow depth data of the years 1991–2023 were selected for the variance and trend analysis as these variables are closely related to the hydrological properties of rivers (Veijalainen et

al., 2010; Irannezhad et al., 2022). Annual min, mean, max, and total values were derived from the daily data and used in the trend analysis (Fig. 4). In addition, duration of snow cover, number of precipitation-days, and occurrence of extreme snow/precipitation events (95th percentile) were derived for the trend analysis. For detailed analysis of spring-time trends, the corresponding measures were also derived for March, April, and May. Only one weather station was included in the analysis as other stations are located 50–100 km away with over 100 m elevation difference to the area of interest. The year 1991 was included in the climate time series as the analysis was conducted on hydrological years rather than calendar years.

The M–K trend test was carried out on all climate variables with an $\alpha = 0.05$ significance level to identify statistically significant monotonic trends. In addition to climate variables, the M–K trend test was run on the classified flood hydrographs to examine trends in the occurrence interval, timing, volume, and duration of each flood-event hydrograph type. Possible serial correlations were removed by using Hamed and Rao (1998) M–K modification which is explained in detail in e.g. Daneshvar Vousoughi et al. (2013) and in Jhajharia et al. (2014). The effect of outliers on the trend was removed by using a non-parametric linear regression Sen’s slope estimator (Sen, 1968). Analysis of variance (ANOVA) with $\alpha = 0.05$ significance level was run to identify possible significant differences between the means of the variables, i.e. whether the annual/cold-season/spring or May weather conditions differ significantly across the four spring flood-event type.

3.4 Sediment and bedload sampling

Grab samples taken using the Van Veen sediment sampler, and bedload samples with the Helley–Smith sampler were collected from the riverbed. A total of 70 grab samples (ca. 500 g) and 24 bedload transport samples were collected during various discharges from the area of interest. Grab samples were collected across the entire 6 km reach during a single autumn field campaign under low discharge ($4.2 \text{ m}^3 \text{s}^{-1}$) conditions. Samples were taken from the channel bed at the left and right bank of each meander inlet, apex, and outlet. Bedload transport samples were obtained during both spring and autumn campaigns, under varying discharge levels (7.5, 56, and $4.2 \text{ m}^3 \text{s}^{-1}$). Twelve bedload transport samples were

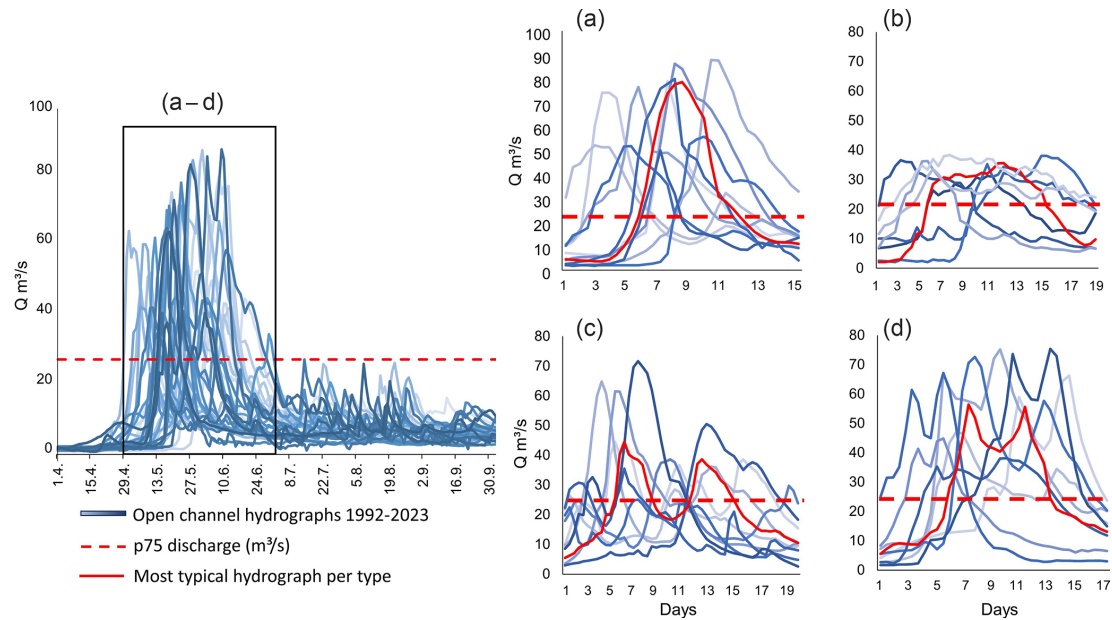


Figure 3. All the generated hydrographs of years 1992–2023. The classification led to four distinct flood-event shapes: (a) High one-peak flood, (b) Low one-peak flood, (c) Flood with two separate peaks, and (d) Flood with a wavy peak. The solid red hydrograph is the most typical flood event of each shape which was thus used in the morphodynamic model. Red dashed line is the 75th percentile threshold discharge for spring flood.

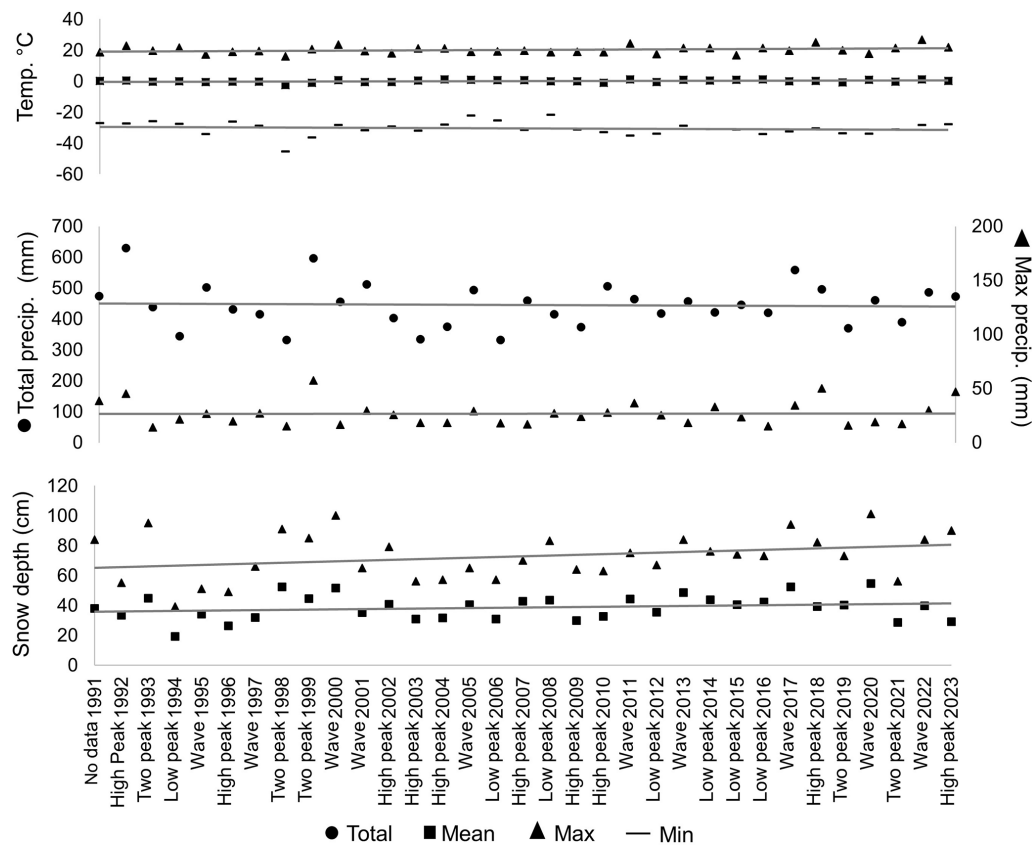


Figure 4. The annual climate time series of the 32-year time period derived from the daily data. The corresponding flood-event types are marked on the x axis.

collected per campaign, each with a sampling duration of 6 min. The samples were dry sieved using half-phi intervals and the amount of material in each sieve was weighted. Sample statistics were calculated in GRADISTAT-program (Blott and Pye, 2001) using the method of moments which is based on a logarithmic distribution of sample phi sizes. GRADISTAT utilizes its own scale with only four classes (Silt, 0.002–0.063 mm, Sand, 0.063–2 mm, Gravel, 2–64 mm, and Boulders 64–2048 mm). The results of sediment and bedload sampling were utilized in the morphodynamic model as multiple sediment fractions, spatially varying Manning's roughness parameter, and for calibrating and validating the sediment transport rates (see details in Blåfield et al., 2024b).

3.5 Morphodynamic modelling

The authors have previously presented and validated the model used in this study (Blåfield et al., 2024b). In this study, four distinct flood-event hydrographs (A–D in Table 2) were simulated using the same initial channel geometry and sediment composition. A depth-averaged morphodynamic model with a curvilinear, unstructured grid of 2×2 m cell size was built utilizing the FLOW 2D-module of Delft3D software. The model geometry was based on a digital elevation model derived from structure from motion (SfM). Specific details of the SfM creation can be found in Blåfield et al. (2024b), and general information from Micheletti et al. (2013), and Dietrich et al. (2017). Multiple sediment fractions and spatially varying Manning's roughness based on the grab sediment samples from the field were used, as these additions have been shown to significantly improve predicted morphodynamics (Kasvi et al., 2015). Each simulation featured hourly varying discharge conditions to evaluate sediment transport dynamics, sediment transport hysteresis patterns, and morphological responses to the shape and sequencing of the simulated hydrographs. The model time step was set to 0.05 min, with both spin-up and output intervals set at 720 min. Morphology, source and sink terms, and total sediment transport were updated at each time step. The model solved morphology independently based on the source and sink terms of van Rijn (1993) approach. Transport boundary conditions, i.e. sediment feeding into the model, were solved using the Neumann law and updated at each time step. This allowed the model to dynamically adjust the sediment supply and concentration at the inflow to match the internal model conditions, thereby minimizing accretion near the model boundaries. Subsequently, sediment transport hysteresis and geomorphic activity for each flood-event type were calculated from the source and sink terms, as well as from the modelled total volume of sediment mobilized within the inundated area. The default scheme for dry-cell erosion of banks was applied without further adjustment, as the focus of the study was on longitudinal sediment transport and vertical changes to the channel bed. Detailed parametrization, as well

as the model's calibration and validation are provided in Blåfield et al. (2024b).

Delft3D is unable to simulate ice-covered flows or the effects of freeze–thaw processes on bank erosion. These limitations, together with the absence of vertical flow representation in the two-dimensional simulation, introduce simplifications into the modelling of flow dynamics and sediment transport. The use of user-defined parameters further contributes to uncertainty, particularly in the spatial and temporal patterns of erosion, transport, and deposition. The van Rijn (1993) approach is sensitive to user-defined parameters such as sediment fraction, composition, and associated threshold conditions (Pinto et al., 2006). However, Kasvi et al. (2015) demonstrated that the van Rijn formulation performs more reliably when applied with spatially variable, field-based sediment fractions and Manning's roughness coefficients rather than uniform values. While the van Rijn transport formula typically produces lower transport rates than other formulations (Schuurman et al., 2013; Kasvi et al., 2015), it remains widely regarded as the most physically based and reliable method (Pinto et al., 2006; Kasvi et al., 2015). The user-defined parametrization used in the present study is detailed in Blåfield et al. (2024b). Spatial variability in sediment grain size and Manning's roughness, alongside the inclusion of medium transverse bed slope effects, were identified as key parameters influencing sediment load predictions and morphological change (Nicholas, 2013; Kasvi et al., 2015), and were prioritized for refinement during simulation.

4 Results

4.1 Hydroclimatic conditions and flood-event type variability

The variance analysis of flood events of types A–D and the prevailing climatic conditions indicated that the climatic conditions of the preceding hydrological year were the most significant of the tested variables influencing the type of spring flood event (Table 3). Other significant factors influencing the flood-event type included the cold season (October–May) mean temperature, spring rainfall (March–May), and May warmth, expressed as the cumulative temperature sum in May (Table 3). In addition to climatic conditions, the timing of peak discharge varied significantly between event types. The number of snow cover days in May demonstrated a trend approaching statistical significance (Table 3). By contrast, rainfall during the cold season, May rainfall, and the spring mean temperature did not exhibit significant differences between flood-event types (Table 3).

Flood events of Type A were typically associated with high annual snow accumulation, low annual temperatures, and rapid warming in May, resulting in a low number of snow cover days during May (Fig. 6). These events also experienced high annual precipitation but low spring rainfall (Fig. 6). Thus, flood events of Type A can be charac-

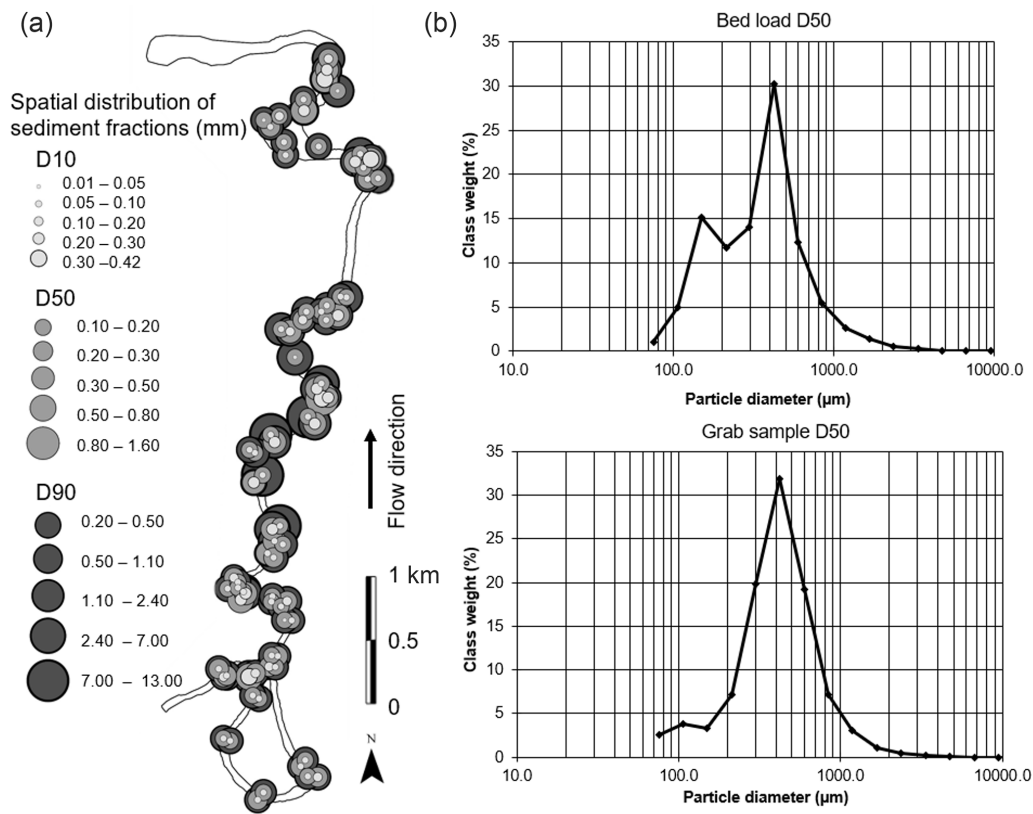


Figure 5. (a) Spatial distribution of sediment fractions D10, D50 and D90 based on the collected field samples. (b) D50 particle diameter distribution of all the collected bedload and grab samples in micrometres.

Table 2. The details of each model run. The flow conditions of flood-events A–D are based on the hydrograph classification in Sect. 3.2. The morphological parameters are based on the sediment and bedload sampling from the field.

Event	Duration (days)	Peak $Q\text{ m}^3\text{ s}^{-1}$	Total Q Volume m^3	Sediment Supply	Morphology	Sediment Composition
A	7	80	29 868 586	Feeding	Sand bed	Sand, Gravel
B	13	35	34 851 505	Feeding	Sand bed	Sand, Gravel
C	14	48	26 238 345	Feeding	Sand bed	Sand, Gravel
D	9	60	31 201 609	Feeding	Sand bed	Sand, Gravel

terized as occurring in cold, snow-rich years, where rapid warming in May leads to sharp and high flood hydrographs. Flood events of Type B were associated with the warmest cold season mean temperatures, along with moderate spring rainfall, snow accumulation, and cumulative May temperatures (Fig. 6). These conditions suggest that snowmelt may begin during the cold season and continue through spring, resulting in reduced energy availability during the main melt period in May. Flood events of Type C were linked to the lowest annual precipitation, the lowest cold season temperatures, and the coldest May temperatures (Fig. 6). However, these events also exhibited the highest snow accumulation during spring. Overall, Type C floods reflect dry, mixed, or transitional climatic conditions, in which a particularly cold

winter and spring lead to delayed snowmelt. This delayed melt, when combined with May rainfall and variable temperatures, may result in two distinct melt peaks. Flood events of Type D were characterized by high annual and spring snow accumulation, alongside the warmest annual and cold season mean temperatures, but relatively low temperatures in May, leading to a prolonged persistence of snow cover during May. These events also experienced high annual precipitation and considerable variation in spring rainfall. Consequently, this flood type typically occurs following a warm and wet year, when May is cold and experiences highly variable rainfall, resulting in non-uniform snowmelt and the development of wavy hydrographs.

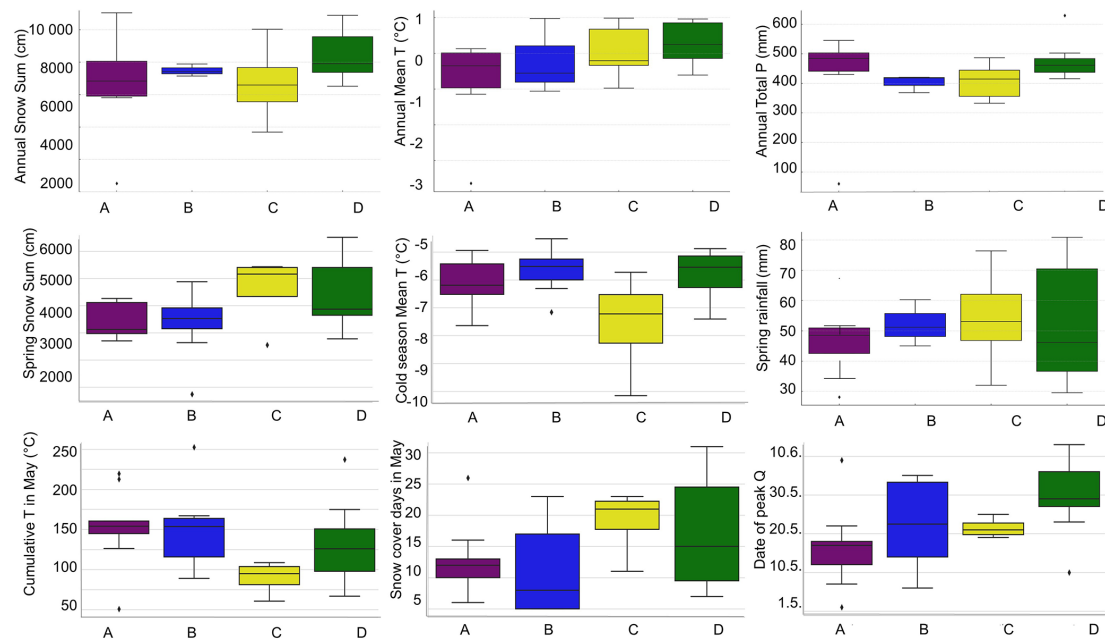


Figure 6. Statistically significant differences between the variable means illustrated in the boxplots, showing the distribution, median, and variation of climate variables associated with each flood-event type. Two borderline variables close to significance (May snow cover days and spring snow sum) were plotted as well.

Table 3. Results of one-way ANOVA test on the main variables with $\alpha = 0.05$ significance level. Statistically significant p values are bolded. T = temperature, P = precipitation, cold season = October–May, spring = March, April, May.

Variable	F statistics	p value
Annual mean T	3.73	0.022
Annual snow sum	7.73	0.006
Annual total P	4.00	0.017
Cold season mean T	3.38	0.032
Cold season rainfall	2.26	0.104
Spring mean T	1.78	0.174
Spring snow sum	1.93	0.103
Spring rainfall	3.13	0.050
May cumulative T	3.41	0.032
May no. of snow cover days	2.36	0.083
May rainfall	0.97	0.420
Peak Q timing	3.28	0.035

The wavy (D) and high one-peak (A) events appeared the most frequently, both occurring 10 times within the 32-year time series. The wavy events of type D had an average duration of 9 d whereas the high one-peak event of type A lasted 7 d on average. Low one-peak events of type B occurred 7 times and had the longest average duration of 13 d. Finally, the two-peak events of type C were the least frequent type with only five occurrences lasting 14 d on average. No significant trends were observed in occurrence interval, duration, volume, or timing of any of the flood-event

types within the 32-year time series (Fig. 7). Trend analysis on the climate variables indicate that in snow-related variables (mean, maximum, and extreme snow), all annual trends (square marker) were positive with a statistically significant increase. The maximum snow amount showed a statistically significant trend also in spring (March–May, circle marker). The number of snow days, however, showed a non-significant weakly negative trend (Fig. 7). Temperature trends were mostly positive, with statistically significant increases in both annual and spring mean temperature (Fig. 7). Springtime maximum temperature had a significant increasing trend indicating that springs, in particular, have become warmer over the time series. Minimum temperature showed a non-significant trend in annual and springtime data. Precipitation-related trends were more variable. Mean and maximum precipitation exhibited mostly negative non-significant trends or no trend at all, while the annual extreme precipitation (95th percentile) showed a significant decreasing trend (Fig. 7). Even though the springtime precipitation did not indicate significant trends in volume, the number of precipitation days showed a significant increasing trend.

Overall, the results suggest that while the frequency and characteristics of individual flood-event types have remained relatively stable over the 32-year period, underlying climatic drivers have undergone notable changes. In particular, the increase in snow accumulation and rising spring temperatures point toward a shift in the timing and dynamics of snowmelt, even if not yet reflected in observable flood trends. The significant rise in the number of precipitation days dur-

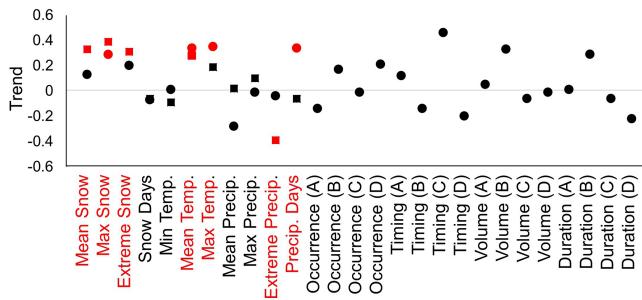


Figure 7. The M-K-trend test results of the climate-related variables during the 32-year study period. Red markers indicate statistically significant trends and black markers non-significant. Square markers represented annual trends, while circles represent seasonal trends in spring (March–May).

ing spring, despite no clear trend in total precipitation volume, may also contribute to more fragmented or prolonged runoff events, potentially supporting the occurrence of events of type B and D.

4.2 Morphological response to sediment transport hysteresis

The modelled results suggest that hydrograph shape may have a significant influence on morphological response and sediment transport hysteresis. Both the total transported sediment (TTS) and the type of sediment transport hysteresis appeared to vary across the modelled events. The wavy event (Type D) was associated with the largest volume of TTS, with the first peak contributing approximately 59 % and the second peak 41 % of the event's TTS. Thus, the transport rate during the first peak was approximately 28 % higher than during the second peak. In the flood event characterized by two separate peaks (Type C), the first peak contributed 63 % and the second 37 % of the total TTS. Consequently, the transport rate during the second peak was approximately 42 % lower than during the first. The TTS of event C was approximately 17 % lower than that of event D. The high one-peak event (Type A) yielded a TTS volume approximately 4 % lower than event D and approximately 11 % higher than that of event C. In contrast, the low one-peak event (Type B) exhibited a TTS volume approximately 30 % lower than that of the high one-peak event (Type A), and approximately 20 %–32 % lower than the double-peaking events C and D, respectively.

All events predominantly exhibited anticlockwise sediment transport hysteresis, where the transport peak occurred after the peak discharge (Fig. 8a–d), suggesting that sediment transport lagged behind changes in discharge and flow conditions. However, the modelled sediment transport hysteresis loops appeared to vary in complexity and shape depending on the flood-event type. The single-peak events (Types A and B) displayed relatively simple anticlockwise loop-shaped hys-

teresis, with sediment transport following the peak discharge (Fig. 8a–b). Event C appeared to exhibit a more complex hysteresis pattern, including multiple anticlockwise loops, which may indicate that sediment mobilized during the first peak was partially deposited between the peaks, as the second peak showed significantly lower TTS (Fig. 8c). In the wavy event (Type D), the first peak exhibited anticlockwise hysteresis, whereas sediment transport during the second peak appeared to precede the second discharge peak, resulting in clockwise hysteresis (Fig. 8d). This complexity may reflect variability in sediment mobilization processes and sediment availability. Across all events, higher TTS values were observed during the falling limb compared to the rising limb at corresponding discharge values, suggesting that sediment transport was not directly proportional to discharge (Fig. 8a–d). This discrepancy highlights the potential influence of delayed and progressive sediment mobilization, as well as the lagged morphological response of bedforms. These findings imply that flood-event shape may have a considerable influence on sediment transport hysteresis and, consequently, on riverbed morphological development.

Each modelled event appeared to demonstrate different patterns of morphological response (Fig. 9a–d), influenced by variations in sediment transport hysteresis, stream power, and flow velocity. Event A produced the second highest total volume of mobilized sediment and geomorphic activity (Fig. 9a). Based on the model, this event appeared to experience the most extensive erosion throughout the reach, with deposition areas remaining relatively localized. The highest stream power values were modelled in this event, exceeding 24 W m^{-2} , alongside a mean flow velocity of 0.61 m s^{-1} , both of which probably contributed to substantial erosion and an overall net sediment loss of $-14\,772 \text{ m}^3$. Sediment input from upstream was insufficient to compensate for this loss. In contrast, event B exhibited the lowest geomorphic activity, with a more balanced distribution of erosion and deposition across the river reach, resembling classical meander behaviour with distinct riffles and pools (Fig. 9b). Stream power during this event was considerably lower, predominantly below 10 W m^{-2} , with a mean flow velocity of 0.36 m s^{-1} . These conditions probably facilitated the deposition of eroded and transported sediment within the reach, resulting in a net sediment gain of 5482 m^3 .

Event C showed a relatively balanced response, with an even distribution of erosion and deposition, and the smallest net change, resulting in a sediment gain of 1132 m^3 (Fig. 9c). The upstream section experienced the greatest erosion, while sediment accumulation was most pronounced downstream. Only minor changes occurred in the middle reach based on the model. Stream power for event C was moderate, with values mostly below 16 W m^{-2} and only with occasional exceedances above 20 W m^{-2} . Event D exhibited the most fragmented morphological response, with small, scattered areas of both erosion and deposition distributed throughout the reach (Fig. 9d). The stream power distribution for event D

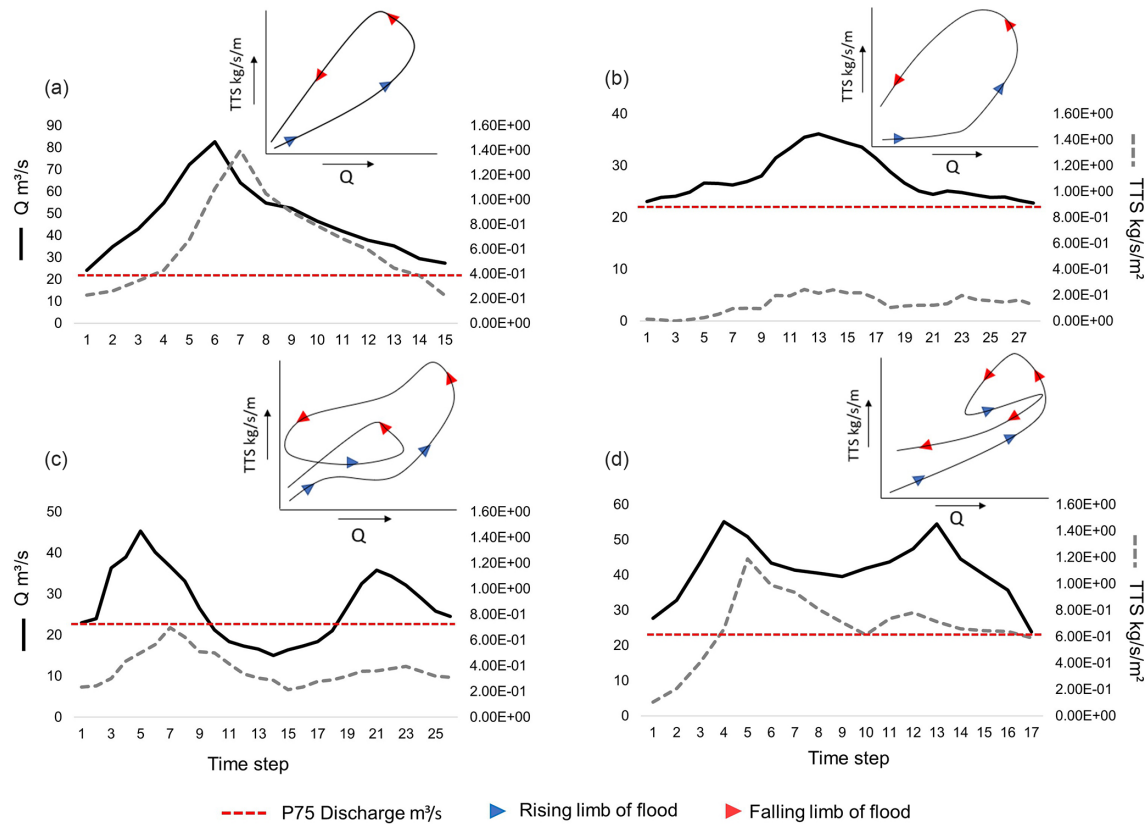


Figure 8. The modelled flood-event hydrographs and sediment load at each time step. On the upper right corner of each graph is the sediment transport hysteresis of the event type. The blue arrows indicate rising limb and red arrows falling limb of the flood. The red dashed line shows the threshold p90 discharge. (a) High one-peak event and sharp anticlockwise sediment transport hysteresis. (b) low one-peak event and wide anticlockwise sediment transport hysteresis. (c) Event with two separate peaks and anticlockwise sediment transport hysteresis with a loop. (d) Wavy type event and hysteresis loop with anticlockwise and clockwise directions.

was more similar to that of event A, with values exceeding 20 W m^{-2} and a mean flow velocity of 0.54 m s^{-1} . Despite the relatively high energy, event D produced a more balanced sediment budget, though it still resulted in a net sediment loss of -6267 m^3 . Geomorphic activity per unit area appeared highest for events A and D, both of which showed considerable sediment mobilization but resulted in different morphological responses probably due to hydrograph shape. Events B and C exhibited lower geomorphic activity, with a tendency towards sediment deposition rather than erosion. The pattern of morphological change associated with the modelled flood events thus appeared to be linked to the peak shape, sequencing, and the resulting sediment transport hysteresis patterns, which collectively influenced the morphological response of bedforms.

5 Discussion

5.1 Flood-event types and hydroclimatic conditions

The results of variance analysis and trend test of climate variables and flood-event types aligned with well-documented

responses to climate change in cold regions (Cockburn and Lamoureux, 2008; Vormoor et al., 2016; Matti et al., 2017; Arp et al., 2020). The significant increase in both mean and maximum spring temperatures matched global climate model predictions for continued warming at high latitudes (Koenig and Brodeau, 2017; Huo et al., 2022). The increased snow depth also aligned with Pulliainen et al. (2020), who reported rising snow accumulation and snow water equivalent in the studied region. Despite this, no significant changes in flood volumes were observed, consistent with previous studies in Fennoscandia (Veijalainen et al., 2010; Korhonen and Kuusisto, 2010; Matti et al., 2017; Lintunen et al., 2024). This lack of change was attributed to milder winter conditions and longer snowmelt period resulting from warming temperatures, which lead to more stable runoff during spring (Fischer and Schumann, 2020; Zhang et al., 2023). Additionally, no significant trends were found in the timing, duration, or interval of flood events, consistent with earlier research in snowmelt-dominated regions (Veijalainen et al., 2010; Vormoor et al., 2016; Matti et al., 2017).

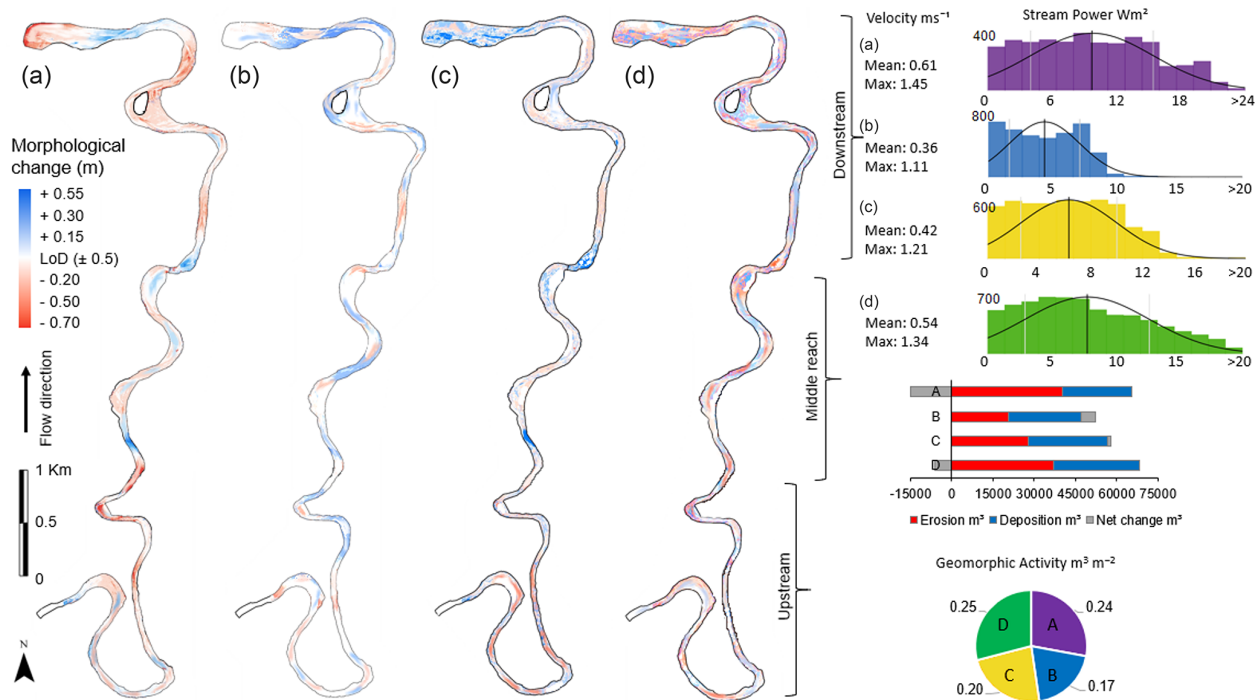


Figure 9. Morphological adjustment of each flood-event (A–D) in left panel: (a) Distinct areas of heavy erosion and deposition. (b) Desecrate morphological changes but distinct areas of erosion and deposition. (c) More complex morphological changes patched around the river reach. (d) Heavy erosion and deposition spread complexly inside the reach. Right panel: A–D events mean and maximum velocity, histograms of stream power (x) distribution within number of model cells (y), volume of erosion, deposition, and net change, and geomorphic activity.

Despite the absence of significant trends, low-peak floods (B) increased in both volume and duration, while wavy floods (D) showed a reduction, respectively. Based on the results of ANOVA, both flood events of this type were influenced by high annual temperature and high snow accumulation, but significantly different springtime and May weather conditions. Events of type B experienced long and warm melt period during spring whereas events of type D were associated with late spring warmth with varying amounts of rainfall leading to non-uniform runoff. The climatic conditions associated with these event types are expected to intensify across the Northern Hemisphere (Callaghan et al., 2011; Kunkel et al., 2016; Connolly et al., 2019; Pulliainen et al., 2020; Hu et al., 2024), although climate change effect on snow accumulation is likely to vary spatially. These event types also exhibited an increase of occurrence interval indicating that these flood-event types are likely to become more common in the future. High one-peak floods (A), however, were associated with cold, snow-rich years, where rapid warming in May leads to sharp and high flood hydrographs. This is consistent with findings that cold springs delay snowmelt and ground thaw, leading to high discharge peaks when the thaw eventually occurs (Labuhn et al., 2018). Unlike double-peaking floods, single-peak events involved lower temperatures and rainfall during spring, and therefore the rain-on-snow effect could be linked to the wetter conditions typical to events of

type D. Even though events of type C are also double peaking, these hydrographs were linked to dry, mixed, or transitional climatic conditions, in which a particularly cold winter and spring lead to delayed snowmelt. Hydrographs of event type C had, however, a significant amount of rainfall in May which together with cold temperature conditions probably causes the two separate melt peaks typical to this event.

Climate change is expected to increase annual temperatures and to modify the precipitation patterns in high-latitude areas (Zhang et al., 2023; Blöschl et al., 2017). These changes will probably have an effect on the occurrence of certain flood-event types. Increased spring rainfall can increase rain-on-snow events significantly amplifying runoff and flood peaks, particularly together with deep snow packs and accelerated snowmelt from warmer spring temperatures. Similar pattern have been recognized previously on high-latitudes by Fischer and Schumann (2020). The results observed in this study point to the direction of possible future hydroclimatic regime shift. These findings highlight the complex effects of climate change on flood events and underscore the importance of considering flood-event sequencing in assessing the effects of hydroclimatic shifts. Future research could explore climate teleconnections, such as the North Atlantic Oscillation (NAO) or Arctic Oscillation (AO), to better understand the conditions driving specific flood events (Dahlke et al., 2012; Villarini et al., 2014; Irannezhad et al.,

2022). In addition, we note that while interpreting the results of this study, especially the results of ANOVA, the sample size has a critical effect on the reliability and validity of the results. Larger sample sizes increase the statistical power of the test, improving the ability to detect true differences between group means (Lakens, 2022). They also provide more precise estimates of means and variances, reduce the influence of outliers, and help satisfy the assumptions of normality and homogeneity of variances. In contrast, small samples can result in underpowered tests, unstable F-statistics, and greater sensitivity to assumption violations, ultimately reducing the robustness of the findings

5.2 Flood-event types and morphological response

When interpreting the morphological results of the simulations in this study some limitations should be considered. As a depth-averaged model, it did not resolve vertical flow structures or secondary currents, which limit the capacity to fully represent sediment transport and bank erosion processes (Pinto et al., 2006; Nicholas, 2013; Williams et al., 2016). In addition, the model lacks the ability to simulate ice-covered flows and freeze–thaw effects, both of which significantly influence sediment dynamics and channel stability in cold-region rivers (Zhang et al., 2022). Model sensitivity to user-defined parameters, such as sediment fractions and roughness coefficients, further contributes to output uncertainty (Pinto et al., 2006). Moreover, the use of morphological acceleration factors and simplified boundary conditions may exaggerate or underrepresent morphological processes. Consequently, while the simulation runs presented in this study are effective in assessing relative differences between scenarios, caution is necessary when interpreting absolute sediment budgets and localized morphological changes due to simplifications, and the fact that it cannot simulate ice and freeze–thaw effect on sediment transport and bank erosion.

Nevertheless, the model simulations showed that the channel bed's morphological response was influenced by flood-event type and sequences, as well as sediment transport hysteresis pattern, rather than just flood magnitude. Similar findings have been made by Kasvi (2015) who found that the flood duration and flow characteristics have a notable effect on channel morphology. All events exhibited dominant anticlockwise hysteresis, common in sand-bed rivers with upstream sediment supply and bedload-dominated transport (Tananaev, 2015; Gunsolus and Binns, 2018). However, the riverbed's morphological response varied depending on the modelled hydrograph shape. Single-peak events (A and B) produced distinct erosion and deposition patterns, while double-peaking events (C and D) led to fragmented, small-scale morphological features. Particularly, event B formed classic riffles and pools, typical to meandering rivers (Hooke, 2003; Salmela et al., 2022), whereas the reduced sediment transport during second peaks in double-peaking events, also

noted in previous flume experiments (Martin and Jerolmack, 2013; Mao, 2018), resulted in more complex, small-scale bedforms.

The reduction in sediment transport during the second flood peak has been previously attributed to bed surface reorganization, including coarser sediment exposure (armouring) and infiltration of finer sediments (kinetic sieving), which stabilizes the bed, requiring more energy for remobilization (Curran and Waters, 2014; Dudill et al., 2017; Ferdowsi et al., 2017; Mao, 2018). However, event D displayed clockwise hysteresis during the second peak, suggesting that the riverbed was not able to stabilize between the peaks, enabling faster remobilization of sediments during the second peak and therefore higher TTS compared to other flood events. This can also be a sign of finer sediment contribution due to bank erosion as bank erosion and slumping/mass failures increase as the WL decreases (Lotsari et al., 2014; Lotsari et al., 2024; Yang et al., 2024). This is further affected by freeze–thaw cycles and seasonally frozen ground, events that the model used in this study cannot replicate. Whether the bank or bars are frozen during the rising, peaking, and falling limb of the flood has significant effect on the amount of erosion (Lotsari et al., 2024; van Rooijen and Lotsari, 2024; Yang et al., 2024) as thawing banks have higher erosion magnitude compared to frozen banks. In addition, the moisture content and amount of freeze–thaw cycles affects the erodibility of the soil by reducing bank stability (Li et al., 2022; Lotsari et al., 2024). This is a factor which probably has significant effect on bank erosion rates and sediment flux volumes in the future as previous studies have noted that the freeze–thaw cycles are prolonged due to climate change (Blåfield et al., 2024a; Sha et al., 2025). In addition to prolonged freeze–thaw cycle, increased cold season discharge and earlier freshet occurring under warmer conditions enhance river-bank erosion in most areas (Brown et al., 2020).

The fragmented bedforms from double-peaking floods were probably caused by secondary bedforms cannibalizing the larger topography from the first peak, a phenomenon observed in flume studies (Wilbers and Ten Brinke, 2003; Martin and Jerolmack, 2013). In addition to flood hydrograph shape and hysteresis pattern, sediment particle size played a key role in morphological adjustment. The middle reach with the largest particles (Fig. 5) was eroded mainly during events A and D, while events B and C caused minimal change in this section of the river. This finding was consistent with earlier research on particle size effect on sediment transport hysteresis and remobilization of the sediment particles (Mao, 2012; Malutta et al., 2020). Despite variations in the modelled runoff volumes, the study identified distinct morphological response patterns for each flood-event type. These patterns, shaped by sediment transport hysteresis, distribution of sediment particle size, and flood-event sequences, align with findings from previous studies (Martin and Jerolmack, 2013; Gunsolus and Binns, 2018; Mao, 2018). The results highlighted the crucial role of different flood-event types in shap-

ing river morphology, revealing that, while event variation probably helps maintain channel equilibrium in the long-term, prolonged exposure to certain events – such as high-energy or multi-peaking floods – could disrupt this balance. Such evolution have the potential to destabilize the channel, by altering sediment connectivity, transport processes, and ultimately the morphological structure of the river systems (Bracken et al., 2015; Zhang et al., 2023). Understanding these responses is essential for predicting future river behaviour and managing morphological stability.

5.3 Forecasted hydroclimatic shift and long-term morphological adjustment

This study highlighted the importance of understanding how fluvial sand and gravel-bed systems respond to climatic conditions, particularly by examining the sequences of flood hydrographs, which are often overlooked, and more focus is paid on factors like flood volume, timing, or frequency. The results revealed that flood-event type and peak sequencing had significant effect on the morphological response of the channel. This together with the observed trends, suggested that even in regions, like the one studied, where hydroclimatic changes are not yet fully visible (Veijalainen et al., 2010; Lintunen et al., 2024), flood-event characteristics are evolving with consequences to the river morphology. This and the observed trends in the hydroclimatic variables underscores that hydroclimatic change is not uniform in space and time across cold regions and rivers should be assessed at the catchment scale to predict future morphological adjustment accurately.

The increase (decrease) of double (single) peaking floods could lead to changes in river system stability, sediment loads, and in the spatial distribution of long-term morphological adjustment if certain type of morphological response begin to accumulate (Bracken et al., 2015; Zhang et al., 2023; Blåfield et al., 2024a). Furthermore, previous research findings suggesting that sediment loads in cold regions could rise by 20 %–30 % for every 1–2 °C increase in temperature (Syvitski et al., 2002; Li et al., 2021) was supported by this study, as the double-peaking floods related to warmer annual temperatures, showed higher geomorphic activity and sediment loads compared to single peaking events of similar volume. The temperature increase together with altered morphological response pattern could eventually lead to sediment transport regime shift. However, the anticipated shift is likely to be a gradual process (Zhang et al., 2023), and the river system may eventually stabilize again. Yet, before stabilizing the shift is likely to challenge the river channel stability, making long-term morphological adjustment, such as meander migration, less predictable (Wohl, 2017; Hopwood et al., 2018).

Shifts in the sediment transport regime, along with changes in morphological response and long-term adjustment to evolving flood patterns, are likely to influence the

morphological response to summer and autumn precipitation by altering sediment availability and bed form composition. Although these precipitation peaks were not the focus of this study, these seasonal peaks should be considered when predicting and evaluating long-term morphological adjustment of river channels as the distribution of seasonal sediment load is probably shifting towards summer and autumn peaks (Li et al., 2021; Zhang et al., 2023; Blåfield et al., 2024a). This could have significant implications for river ecosystems, flood risk management, and infrastructure planning (Beel, et al., 2021; Gupta et al., 2022; Najafi et al., 2021). As discharge regimes become increasingly event-driven rather than seasonally predictable, traditional models of sediment flux that assume clear seasonal patterns may no longer be applicable. Hysteresis patterns, where sediment concentration and water discharge are no longer linearly related, can reveal critical thresholds, sediment sources, and system memory that are key to predicting future river behaviour. Therefore, future research should focus on understanding the combined effects of flood-event sequencing, changing precipitation patterns, and sediment transport dynamics under evolving climatic conditions. Long-term monitoring and advanced modelling efforts will be essential to predict the future morphological adjustments of rivers and to develop strategies for mitigating the effect of these changes on ecological systems.

6 Conclusions

The findings of this study emphasize the critical role that flood-event variability and sequencing play in shaping the morphological response of fluvial sand and gravel-bed systems in cold regions. The results demonstrated that even in areas where hydroclimatic changes are not yet fully visible, flood-event characteristics are evolving and remain closely linked to specific climatic conditions. Each flood-event type produced distinct morphological responses, such as the formation of riffles and pools during single-peaking floods, and more fragmented and irregular bed forms in double-peaking floods. In addition, sediment grain size significantly influenced the spatial distribution of erosion and deposition. The increase of double-peaking flood events, coupled with rising temperatures, could lead to a shift in sediment transport regimes, resulting in heightened geomorphic activity and altered sediment loads. The results underscore the importance of assessing hydroclimatic conditions and flood hydrograph sequences at the catchment scale to accurately predict future morphological adjustment, as the effects of hydroclimatic shift are not uniform across the arctic. Future research should focus on the combined effects of flood sequences, precipitation patterns, and sediment transport dynamics to develop effective strategies for managing the evolving river systems under climate change. These changes are expected to affect long-term river stability, with significant implications for river ecosystems and flood risk management.

Data availability. The climate data are openly available at the Finnish Meteorological Institute (FMI) data service (<https://en.ilmatiiteenlaitos.fi/download-observations>, FMI, 2025). The Polmak discharge station data are openly available at the Norwegian Water Resources and Energy Directorate (<https://sildre.nve.no/station/234.18.0?lang=en>, NVE, 2025) data service. All the other data are available on request.

Author contributions. LB – writing the manuscript, fieldwork, methodology, formal analysis, visualization, funding. CGI – formal analysis, editing the manuscript. PA – fieldwork, data curation, resources, reviewing the manuscript, funding, supervision. EK – fieldwork, reviewing the manuscript, funding, supervision.

Competing interests. The contact author has declared that none of the authors has any competing interests.

Disclaimer. Publisher's note: Copernicus Publications remains neutral with regard to jurisdictional claims made in the text, published maps, institutional affiliations, or any other geographical representation in this paper. While Copernicus Publications makes every effort to include appropriate place names, the final responsibility lies with the authors.

Acknowledgements. The authors would like to thank research assistant Oona Oksanen from the Fluvial and Coastal Research Group (University of Turku) for helping with the data processing and other group members who have participated in the fieldwork.

Financial support. This study was funded by the Kone Foundation (grant no. 202104246), AnthroClimocs (grant no. 355018), and by the European Union's Next Generation EU recovery instrument (RRF) through the following Research Council of Finland projects: HYDRO-RDI-Network (grant no. 337279), GreenDigi-Basin (grant no. 347701), and HYDRO-RI-platform (grant no. 346161). The study also received support from the Flagship Programme funding granted by the Research Council of Finland for Digital Waters – DIWA Flagship (grant no. 359247).

Review statement. This paper was edited by Rebecca Hodge and reviewed by two anonymous referees.

References

- Arp, C. D., Whitman, M. S., Kemnitz, R., and Stuefer, S. L.: Evidence of hydrological intensification and regime change from northern Alaskan watershed runoff, *Geophys. Res. Lett.*, 47, e2020GL089186, <https://doi.org/10.1029/2020GL089186>, 2020.
- Beel, C. R., Heslop, J. K., Orwin, J. F., Pope, M. A., Scheverson, A. J., Hung, J. K. Y., Lafnerière, M. J., and Lamoureux, S. F.: Emerging dominance of summer rainfall driving High Arctic terrestrial-aquatic connectivity, *Nat. Commun.*, 12, 1448, <https://doi.org/10.1038/s41467-021-21759-3>, 2021.
- Blåfield, L., Marttila, H., Kasvi, E., and Alho, P.: Temporal shift of hydroclimatic regime and its influence on migration of a high latitude meandering river, *J. Hydrol.*, 633, 130935 <https://doi.org/10.1016/j.jhydrol.2024.130935>, 2024a.
- Blåfield, L., Calle, M., Kasvi, E., and Alho, P.: Modelling seasonal variation of sediment connectivity and its interplay with river forms, *Geomorphology*, 463, 109346, <https://doi.org/10.1016/j.geomorph.2024.109346>, 2024b.
- Blöschl, G., Hall, J., Parajka, J., Perdigão, R. A., Merz, B., Arheimer, B., and Živković, N.: Changing climate shifts timing of European floods, *Science*, 357, 588–590, <https://doi.org/10.1126/science.aan2506>, 2017.
- Blott, S. J., and Pye, K.: GRADISTAT: a grain size distribution and statistics package for the analysis of unconsolidated sediments. *Earth surface processes and Landforms*, 26, 1237–1248, <https://doi.org/10.1002/esp.261>, 2001.
- Bracken, L. J., Turnbull, L., Wainwright, J., and Bogaart, P.: Sediment connectivity: a framework for understanding sediment transfer at multiple scales, *Earth Surf. Process. Land.*, 40, 177–188, <https://doi.org/10.1002/esp.3635>, 2015.
- Brown, D. R. N., Brinkman, T. J., Bolton, W. R., Brown, C. L., Cold, H. S., Hollingsworth, T. N., and Verbyla, D. L.: Implications of climate variability and changing seasonal hydrology for subarctic riverbank erosion, *Climatic Change*, 162, 1–20, <https://doi.org/10.1007/s10584-020-02748-9>, 2020.
- Callaghan, T. V., Johansson, M., Brown, R. D., Groisman, P. Y., Labba, N., Radionov, V., and Yang, D.: The Changing Face of Arctic Snow Cover: A Synthesis of Observed and Projected Changes, *Ambio*, 40, 17–31, <https://doi.org/10.1007/s13280-011-0212-y>, 2011.
- Cockburn, J. M. and Lamoureux, S. F.: Hydroclimate controls over seasonal sediment yield in two adjacent High Arctic watersheds, *Hydrol. Process.*, 22, 2013–2027, <https://doi.org/10.1002/hyp.6798>, 2008.
- Connolly, R., Connolly, M., Soon, W., Legates, D. R., Cionco, R. G., and Velasco Herrera, V. M.: Northern Hemisphere Snow-Cover Trends (1967–2018): A Comparison between Climate Models and Observations, *Geosciences*, 9, 135, <https://doi.org/10.3390/geosciences9030135>, 2019.
- Curran, J. C., and Waters, K. A.: The importance of bed sediment sand content for the structure of a static armor layer in a gravel bed river, *J. Geophys. Res., Earth Surface*, 119, 1484–1497, <https://doi.org/10.1002/2014JF003143>, 2014.
- Dahlke, H. E., Lyon, S. W., Stedinger, J. R., Rosqvist, G., and Jansson, P.: Contrasting trends in floods for two sub-arctic catchments in northern Sweden – does glacier presence matter?, *Hydrol. Earth Syst. Sci.*, 16, 2123–2141, <https://doi.org/10.5194/hess-16-2123-2012>, 2012.
- Daneshvar Vousoughi, F., Dinpashoh, Y., Aalami, M. T., and Jhajharia, D.: Trend analysis of groundwater using non-parametric methods (case study: Ardabil plain), *Stoch. Environ. Res. Risk Assess.*, 27, 547–559, <https://doi.org/10.1007/s00477-012-0599-4>, 2013.
- Dietrich, J. T.: Bathymetric structure-from-motion: Extracting shallow stream bathymetry from multi-view stereo photogrammetry, *Earth Surface Processes and Landforms*, 42, 355–364, <https://doi.org/10.1002/esp.4060>, 2017.

- Dudill, A., Frey, P., and Church, M.: Infiltration of fine sediment into a coarse mobile bed: a phenomenological study, *Earth Surface Processes and Landforms*, 42, 1171–1185, <https://doi.org/10.1002/esp.4080>, 2017.
- Favaro, E. A., and Lamoureux, S. F.: Downstream patterns of suspended sediment transport in a High Arctic river influenced by permafrost disturbance and recent climate change, *Geomorphology*, 246, 359–369, <https://doi.org/10.1016/j.geomorph.2015.06.038>, 2015.
- Ferdowsi, B., Ortiz, C. P., Houssais, M., and Jerolmack, D. J.: Riverbed armouring as a granular segregation phenomenon, *Nature communications*, 8, 1363, <https://doi.org/10.1038/s41467-017-01681-3>, 2017.
- Fischer, S. and Schumann, A.: Spatio-temporal consideration of the impact of flood-event types on flood statistics, *Stoch. Environ. Res. Risk. Assess.*, 34, 1331–1351, <https://doi.org/10.1007/s00477-019-01690-2>, 2020.
- FMI: Download observations, Utsjoki Nuorgam, Finnish Meteorological Institute [data set], <https://en.ilmatieteenlaitos.fi/download-observations> (last access: 24 August 2024), 2025.
- Gisnäs, K., Etzelmüller, B., Lussana, C., Hjort, J., Sannel, A. B. K., Isaksen, K., Åkerman, J.: Permafrost map for Norway, Sweden and Finland, *Permafrost and periglacial processes*, 28, 359–378, <https://doi.org/10.1002/ppp.1922>, 2017.
- Gohari, A., Shahrood, A. J., Ghadimi, S., Alborz, M., Patro, E. R., Klöve, B., and Haghighi, A. T.: A century of variations in extreme flow across Finnish rivers, *Environ. Res. Lett.*, 17, 124027, <https://doi.org/10.1088/1748-9326/aca554>, 2022.
- Gunsolus, E. H. and Binns, A. D.: Effect of morphologic and hydraulic factors on hysteresis of sediment transport rates in alluvial streams, *River Res. Appl.*, 34, 183–192, <https://doi.org/10.1002/tra.3184>, 2018.
- Gupta, H., Reddy, K. K., Gandla, V., Paridula, L., Chiluka, M., and Vashisth, B.: Freshwater discharge from the large and coastal peninsular rivers of India: A reassessment for sustainable water management, *Environ. Sci. Pollut. Res.*, 29, 14400–14417, <https://doi.org/10.1007/s11356-021-16811-0>, 2022.
- Hamed, K. H. and Rao, A. R.: A modified Mann-Kendall trend test for autocorrelated data, *J. Hydrol.*, 204, 182–196, [https://doi.org/10.1016/S0022-1694\(97\)00125-X](https://doi.org/10.1016/S0022-1694(97)00125-X), 1998.
- Hirvas, H., Lagerbäck, R., Mäkinen, K., Nenonen, K., Olsen, L., Rodhe, L., and Thoresen, M.: The Nordkalott Project: studies of Quaternary geology in northern Fennoscandia, *Boreas*, 17, 431–437, <https://doi.org/10.1111/j.1502-3885.1988.tb00560.x>, 1988.
- Hopwood, M. J., Carroll, D., Browning, T. J., Meire, L., Mortensen, J., Krisch, S., and Achterberg, E. P.: Non-linear response of summertime marine productivity to increased meltwater discharge around Greenland, *Nat. Commun.*, 9, 3256, <https://doi.org/10.1038/s41467-018-05488-8>, 2018.
- Hooke, J.: River meander behaviour and instability: a framework for analysis, *T. I. Brit. Geogr.*, 28, 238–253, <https://doi.org/10.1111/1475-5661.00089>, 2003.
- Huo, R., Li, L., Engeland, K., Xu, C. Y., Chen, H., Paasche, Ø., and Guo, S.: Changing flood dynamics in Norway since the last millennium and to the end of the 21st century, *J. Hydrol.*, 613, 128331, <https://doi.org/10.1016/j.jhydrol.2022.128331>, 2022.
- Hu, Y., Che, T., Dai, L., Zhu, Y., Xiao, L., Deng, J., and Li, X.: A long-term daily gridded snow depth dataset for the Northern Hemisphere from 1980 to 2019 based on machine learning, *Big Earth Data*, 8, 274–301, <https://doi.org/10.1080/20964471.2023.2177435>, 2024.
- Ielpi, A., Lapôtre, M. G., Finotello, A., and Roy-Léveillé, P.: Large sinuous rivers are slowing down in a warming Arctic, *Nature Climate Change*, 13, 375–381, <https://doi.org/10.1038/s41558-023-01620-9>, 2023.
- Irannezhad, M., Ahmadian, S., Sadeqi, A., Minaei, M., Ahmadi, B., and Marttila, H.: Peak spring flood discharge magnitude and timing in natural rivers across northern Finland: Long-term variability, trends, and links to climate teleconnections, *Water*, 14, 1312, <https://doi.org/10.3390/w14081312>, 2022.
- Jhajharia, D., Dinpashoh, Y., Kahya, E., Choudhary, R. R., and Singh, V. P.: Trends in temperature over Godavari River basin in Southern Peninsular India, *Int. J. Climatol.*, 34, <https://doi.org/10.1002/joc.3761>, 2014.
- Johansson, P.: Late Weichselian deglaciation in Finnish Lapland, *Applied Quaternary research in the central part of glaciated terrain*, 47, 2007.
- Kärkkäinen, M., and Lotsari, E.: Impacts of rising, peak and receding phases of discharge events on erosion potential of a boreal meandering river, *Hydrological Processes*, 36, <https://doi.org/10.1002/hyp.14674>, 2022.
- Kasvi, E.: Fluvio-morphological Processes of meander bends – combining conventional field measurements, closerange Remote sensing and Computational modelling, *Annales Universitatis Turkuensis, Series IIA*, 298, 2015.
- Kasvi, E., Alho, P., Lotsari, E., Wang, Y., Kukko, A., Hyypä, H., and Hyypä, J.: Two-dimensional and three-dimensional computational models in hydrodynamic and morphodynamic reconstructions of a river bend: sensitivity and functionality, *Hydrol. Process.*, 29, 1604–1629, <https://doi.org/10.1002/hyp.10277>, 2015.
- Karimae Tabarestani, M. and Zarrati, A. R.: Sediment transport during flood-event: a review, *Int. J. Environ. Sci. Technol.*, 12, 775–788, <https://doi.org/10.1007/s13762-014-0689-6>, 2015.
- Kociuba, W.: The Role of Bedload Transport in the Development of a Proglacial River Alluvial Fan (Case Study: Scott River, Southwest Svalbard), *Hydrology*, 8, 173, <https://doi.org/10.3390/hydrology8040173>, 2021.
- Korhonen, J. and Kuusisto, E.: Long-term changes in the discharge regime in Finland, *Hydrol. Res.*, 41, 253–268, <https://doi.org/10.2166/nh.2010.112>, 2010.
- Koenig, T., and Brodeau, L.: Arctic climate and its interaction with lower latitudes under different levels of anthropogenic warming in a global coupled climate model, *Climate Dynamics*, 49, 471–492, <https://doi.org/10.1007/s00382-016-3354-6>, 2017.
- Kunkel, K. E., Robinson, D. A., Champion, S., Yin, X., Estilow, T., and Frankson, R. M.: Trends and Extremes in Northern Hemisphere Snow Characteristics, *Curr. Clim. Change Rep.*, 2, 65–73, <https://doi.org/10.1007/s40641-016-0036-8>, 2016.
- Labuhn, I., Hammarlund, D., Chapron, E., Czymzik, M., Dumoulin, J. P., Nilsson, A., and Von Grafenstein, U.: Holocene hydroclimate variability in central Scandinavia inferred from flood layers in contourite drift deposits in Lake Storsjön, *Quaternary*, 1, <https://doi.org/10.3390/quat1010002>, 2018.
- Lakens, D.: Sample size justification, *Collabra: Psychology*, 8, 33267, <https://doi.org/10.1525/collabra.33267>, 2022.

- Li, C., Yang, Z., Shen, H. T., and Mou, X.: Freeze-Thaw Effect on Riverbank Stability, *Water*, 14, 2479, <https://doi.org/10.3390/w14162479>, 2022.
- Li, D., Overeem, I., Kettner, A. J., Zhou, Y., and Lu, X.: Air temperature regulates erodible landscape, water, and sediment fluxes in the permafrost-dominated catchment on the Tibetan Plateau, *Water Resour. Res.*, 57, <https://doi.org/10.1029/2020WR028193>, 2021.
- Liébault, F., Laronne, J. B., Klotz, S., and Bel, C.: Seasonal bed-load pulses in a small alpine catchment, *Geomorphology*, 398, 108055, <https://doi.org/10.1016/j.geomorph.2021.108055>, 2022.
- Lininger, K. B., and Wohl, E.: Floodplain dynamics in North American permafrost regions under a warming climate and implications for organic carbon stocks: A review and synthesis, *Earth-Science Reviews*, 193, 24–44, <https://doi.org/10.1016/j.earscirev.2019.02.024>, 2019.
- Lintunen, K., Kasvi, E., Uvo, C. B., and Alho, P.: Changes in the discharge regime of Finnish rivers, *J. Hydrol.*, 53, 101749, <https://doi.org/10.1016/j.ejrh.2024.101749>, 2024.
- Lotsari, E., Vaaja, M., Flener, C., Kaartinen, H., Kukko, A., Kasvi, E., and Alho, P.: Annual bank and point bar morphodynamics of a meandering river determined by high-accuracy multi-temporal laser scanning and flow data, *Water Resour. Res.*, 50, 5532–5559, <https://doi.org/10.1002/2013WR014106>, 2014.
- Lotsari, E., Hackney, C., Salmela, J., Kasvi, E., Kemp, J., Alho, P., and Darby, S. E.: Subarctic river bank dynamics and driving processes during the open-channel flow period, *Earth Surf. Process. Land.*, 45, 1198–1216, <https://doi.org/10.1002/esp.4796>, 2020.
- Lotsari, E., de Vet, M., Murphy, B., McLelland, S., and Parsons, D.: Defrosting river banks: morphodynamics and sediment flux, *EGU General Assembly 2024*, Vienna, Austria, 14–19 Apr 2024, EGU24-10175, <https://doi.org/10.5194/egusphere-egu24-10175>, 2024.
- Luoto, M., Heikkinen, R. K., and Carter, T. R.: Loss of palustrine mires in Europe and biological consequences, *Environ. Conserv.*, 31, 30–37, <https://doi.org/10.1017/s0376892904001018>, 2004.
- Malutta, S., Kobiyama, M., Borges Chaffe, P.-L., and Bernardi Bonumá, N.: Hysteresis analysis to quantify and qualify the sediment dynamics: state of the art, *Water Sci. Technol.*, 81, 2471–2487, <https://doi.org/10.2166/wst.2020.279>, 2020.
- Mansikkaniemi, H.: Geomorphological analysis of Pulmanki-Tana valley in Lapland, *Instituti Geographici Universitatis Turkuensis*, <http://pascal-francis.inist.fr/vibad/index.php?action=getRecordDetail&idt=GEODEBRGM7018012628>, 1967.
- Mao, L.: The effect of hydrographs on bed load transport and bed sediment spatial arrangement, *J. Geophys. Res.*, 117, F03024, <https://doi.org/10.1029/2012JF002428>, 2012.
- Mao, L.: The effects of flood history on sediment transport in gravel-bed rivers, *Geomorphology*, 322, 196–205, <https://doi.org/10.1016/j.geomorph.2018.08.046>, 2018.
- Matti, B., Dahlke, H., Dieppois, B., Lawler, D., and Lyon, S.: Flood seasonality across Scandinavia – Evidence of a shifting hydrograph?, *Hydrol. Process.*, 31, 4354–4370, <https://doi.org/10.1002/hyp.11365>, 2017.
- Martin, R. L. and Jerolmack, D. J.: Origin of hysteresis in bed form response to unsteady flows, *Water Resour. Res.*, 49, 1314–1333, <https://doi.org/10.1002/wrcr.20093>, 2013.
- Meriö, L. J., Ala-aho, P., Linjama, J., Hjort, J., Kløve, B., and Marttila, H.: Snow to precipitation ratio controls catchment storage and summer flows in boreal headwater catchments, *Water Resour. Res.*, 55, 4096–4109, <https://doi.org/10.1029/2018WR023031>, 2019.
- Micheletti, N., Chandler, J., and Lane, S.: Near instantaneous production of digital terrain models in the field using smartphone and Structure-from-Motion photogrammetry, *EGU General Assembly Conference Abstracts*, EGU2013-10501, 2013.
- Najafi, S., Dragovich, D., Heckmann, T., and Sadeghi, S. H.: Sediment connectivity concepts and approaches, *Catena*, 196, 104880, <https://doi.org/10.1016/j.catena.2020.104880>, 2021.
- Nicholas, A. P.: Modelling the continuum of river channel patterns, *Earth Surface Processes and Landforms*, 38, 1187–1196, <https://doi.org/10.1002/esp.3431>, 2013.
- Nikulin, G., Kjellström, E., Hansson, U. L. F., Strandberg, G., and Ullerstig, A.: Evaluation and future projections of temperature, precipitation and wind extremes over Europe in an ensemble of regional climate simulations. *Tellus A: Dynamic Meteorology and Oceanography*, 63, 41–55, <https://doi.org/10.1111/j.1600-0870.2010.00466.x>, 2011.
- NVE: Polmak nye, Sildre [data set], <https://sildre.nve.no/station/234.18.0?lang=en> (last access: 24 August 2024), 2025.
- Pinto, L., Fortunato, A. B., and Freire, P.: Sensitivity analysis of non-cohesive sediment transport formulae, *Continental Shelf Research*, 26, 1826–1839, <https://doi.org/10.1016/j.csr.2006.06.001>, 2006.
- Pulliainen, J., Luojus, K., Derksen, C., Mudryk, L., Lemmetyinen, J., Salminen, M., and Norberg, J.: Patterns and trends of Northern Hemisphere snow mass from 1980 to 2018, *Nature*, 581, 294–298, <https://doi.org/10.1038/s41586-020-2258-0>, 2020.
- Reesink, A. J. and Bridge, J. S.: Evidence of bedform superimposition and flow unsteadiness in unit-bar deposits, South Saskatchewan River, Canada, *J. Sediment. Res.*, 81, 814–840, <https://doi.org/10.2110/jsr.2011.69>, 2011.
- Rimali, A.: Analysing of frozen ground in Finland: affecting environmental factors, trends in northern Finland and applicability of satellite data, <https://urn.fi/URN:NBN:fi:oulu-201903191342>, 2019.
- Salmela, J., Saarni, S., Blåfield, L., Katainen, M., Kasvi, E., and Alho, P.: Comparison of cold season sedimentation dynamics in the non-tidal estuary of the Northern Baltic Sea, *Marine Geology*, 443, 106701, <https://doi.org/10.1016/j.margeo.2021.106701>, 2022.
- Sen, P. K.: Estimates of the regression coefficient based on Kendall's tau, *J. Am. Stat. Assoc.*, 63, 1379–1389, <https://doi.org/10.1080/01621459.1968.10480934>, 1968.
- Seppälä, M.: Distribution of permafrost in Finland, *Bull. Geol. Soc., Finland*, 69, 87–96, 1997.
- Sha, A., Li, D., Walling, D., Zhao, Y., Tian, S., Chen, D., ... and Best, J.: Accelerated river meander migration on the Tibetan Plateau caused by permafrost thaw, *Geophysical Research Letters*, 52, <https://doi.org/10.1029/2024GL111536>, 2025.
- Schuurman, F., Marra, W. A., and Kleinhans, M. G.: Physics-based modeling of large braided sand-bed rivers: Bar pattern formation, dynamics, and sensitivity, *J. Geophys. Res., Earth Surface*, 118, 2509–2527, <https://doi.org/10.1002/2013JF002896>, 2013.
- Sha, A., Li, D., Walling, D., Zhao, Y., Tian, S., Chen, D., ... and Best, J.: Accelerated river meander migration on the Tibetan

- Plateau caused by permafrost thaw, *Geophys. Res. Lett.*, 52, <https://doi.org/10.1029/2024GL111536>, 2025.
- Syvitski, J. P.: Sediment discharge variability in Arctic rivers: implications for a warmer future, *Polar Res.*, 21, 323–330, <https://doi.org/10.3402/polar.v21i2.6494>, 2002.
- Tananaev, N. I.: Hysteresis effects of suspended sediment transport in relation to geomorphic conditions and dominant sediment sources in medium and large rivers of the Russian Arctic, *Hydrol. Res.*, 46, 232–243, <https://doi.org/10.2166/nh.2013.199>, 2015.
- van Rijn, L. C.: Principles of sediment transport in rivers, estuaries and coastal seas, 1993.
- van Rooijen, E. and Lotsari, E.: The spatiotemporal distribution of river bank erosion events and their drivers in seasonally frozen regions, *Geomorphology*, 454, <https://doi.org/10.1016/j.geomorph.2024.109140>, 2024.
- Vatne, G., Takøy Naas, Ø., Skårholen, T., Beylich, A. A., and Berthling, I.: Bed load transport in a steep snowmelt-dominated mountain stream as inferred from impact sensors, *Norsk Geogr. Tidsskr.*, 62, 66–74, <https://doi.org/10.1080/00291950802094817>, 2008.
- Vejjalainen, N., Lotsari, E., Alho, P., Vehviläinen, B., and Käyhkö, J.: National scale assessment of climate change impacts on flooding in Finland, *J. Hydrol.*, 391, 333–350, <https://doi.org/10.1016/j.jhydrol.2010.07.035>, 2010.
- Verdonen, M., Störmer, A., Lotsari, E., Korpelainen, P., Burkhard, B., Colpaert, A., and Kumpula, T.: Permafrost degradation at two monitored palsa mires in north-west Finland, *The Cryosphere*, 17, 1803–1819, <https://doi.org/10.5194/tc-17-1803-2023>, 2023.
- Viglione, A., Chirico, G. B., Komma, J., Woods, R., Borga, M., and Blöschl, G.: Quantifying space-time dynamics of flood-event types, *J. Hydrol.*, 394, 213–229, <https://doi.org/10.1016/j.jhydrol.2010.05.041>, 2010.
- Villarini, G., Goska, R., Smith, J. A., and Vecchi, G. A.: North Atlantic tropical cyclones and US flooding, *Bulletin of the American Meteorological Society*, 95, 1381–1388, <https://doi.org/10.1175/BAMS-D-13-00060.1>, 2014.
- Vormoor, K., Lawrence, D., Schlichting, L., Wilson, D., and Wong, W. K.: Evidence for changes in the magnitude and frequency of observed rainfall vs. snowmelt driven floods in Norway, *J. Hydrol.*, 538, 33–48, <https://doi.org/10.1016/j.jhydrol.2016.03.066>, 2016.
- Wenng, H., Barneveld, R., Bechmann, M., Marttila, H., Krogstad, T., and Skarbøvik, E.: Sediment transport dynamics in small agricultural catchments in a cold climate: a case study from Norway, *Agr. Ecosy. Environ.*, 317, 107484, <https://doi.org/10.1016/j.agee.2021.107484>, 2021.
- Wilbers, A. W. E., and Ten Brinke, W. B. M.: The response of subaqueous dunes to floods in sand and gravel bed reaches of the Dutch Rhine, *Sedimentology*, 50, 1013–1034, <https://doi.org/10.1046/j.1365-3091.2003.00585.x>, 2003.
- Williams, G. P.: Sediment concentration versus water discharge during single hydrologic events in rivers, *J. Hydrol.*, 111, 89–106, [https://doi.org/10.1016/0022-1694\(89\)90254-0](https://doi.org/10.1016/0022-1694(89)90254-0), 1989.
- Williams, R. D., Brasington, J., and Hicks, D. M.: Numerical modelling of braided river morphodynamics: Review and future challenges, *Geography Compass*, 10, 102–127, <https://doi.org/10.1111/gec3.12260>, 2016.
- Wohl, E.: Connectivity in rivers, *Prog. Phys. Geogr.*, 41, 345–362, <https://doi.org/10.1177/0309133317714972>, 2017.
- Yang, J., Jia, D., Zhai, B., Chen, X., and Wang, J.: Bank erosion under the impacts of fluvial erosion, frost heaving/freezing-thaw process of rivers in seasonal frozen regions, *Heliyon*, 10, <https://doi.org/10.1016/j.heliyon.2024.e37448>, 2024.
- Zhang, T., Li, D., Kettner, A. J., Zhou, Y., and Lu, X.: Constraining dynamic sediment-discharge relationships in cold environments: The sediment-availability-transport (SAT) model, *Water Resour. Res.*, 57, e2021WR030690, <https://doi.org/10.1029/2021WR030690>, 2021.
- Zhang, T., Li, D., East, A. E., Walling, D. E., Lane, S., Overeem, I., and Lu, X.: Warming-driven erosion and sediment transport in cold regions, *Nat. Rev. Earth Environ.*, 3, 832–851, <https://doi.org/10.1038/s43017-022-00362-0>, 2022.
- Zhang, T., Li, D., East, A. E., Kettner, A. J., Best, J., Ni, J., and Lu, X.: Shifted sediment transport regimes by climate change and amplified hydrological variability in cryosphere-fed rivers, *Sci. Adv.*, 9, 45, <https://doi.org/10.1126/sciadv.adi5019>, 2023.